The Usage of Muon Tomography in Inspecting the Fukushima Daiichi Nuclear Reactor Cores

Author: Amin Uddin Ahmed
Supervisor: Dr Teppei Katori

Queen Mary University of London,
School of Physics and Astronomy
Mile End Rd, London E1 4NS, UK

We discuss and explore the method for imaging of hazardously radioactive zones via the use of cosmic rays, the process which is described as muon tomography. In particular when other methods cannot be utilised due to excessive risk to personnel, or due to heavy radioactive degradation of common methods of imaging such as camera/digital pictures. This paper focuses on the detector used at Fukushima, and the process via which the emerging technology for building a three dimensional model of the observed enclosed space using long term cosmic muon detection and their interaction with the matter inside the detection zone of interest.

Contents

1 Introduction

1.1 Fukushima Daiichi disaster

On Friday 11th March 2011, at 14:46 Japan Standard Time, a megathrust type earthquake of magnitude 9.0 occurred undersea off the west coast of Japan. The epicentre was approximately 70km west of the Oshika peninsula of Tohoku, and around 30 km under sea level (Figure 1). This very powerful earthquake triggered a tsunami, with maximum wave heights reaching as much as 41 metres, and also travelling over 10 kilometres inland. It took 50 minutes to arrive at Fukushima, and at this point was 14 metres high. Unfortunately, the seawall built to protect the reactor site was only 10 metres high (*1*).

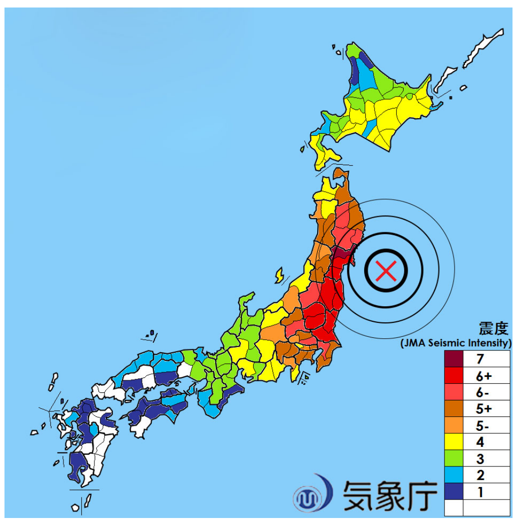

Figure 1: Map of Japan indicating the seismic intensity of the earthquake from the epicentre. (*2*)

The Fukushima nuclear power plant consisted of 6 BWRs (Boiling Water Reactors). Reactors 4, 5, and 6 were already shutdown at the time in order to refuel. Immediately upon receiving news of the earthquake and tsunami, the other reactors 1, 2, and 3 were shut down by insertion of control rods. Thereafter the emergency diesel generators were activated to cool down the fuel rods, which still produce decay heat from the nuclear reaction. The tsunami then arrived and flooded and damaged all the emergency generators of reactors 1-5, while the two generators for reactor 6 remained intact.

Once the emergency diesel generators were flooded, there was no more cooling for the reactors. The temperature of the fuel rods began to rise as the heat was trapped. This would lead to disasters in more than one way: the fuel rods were covered by zirconium cladding. At very high temperatures (around 1500K) zirconium reacts with steam with the chemical reaction: $Zr + 2H_2O \rightarrow ZrO_2 + 2H_2$. This is what occurred in reactors 1-3, releasing around 800-1000 kilograms of pressurised hydrogen gas, which escaped the reactors through ventilation, rose to the top of the buildings and came into contact with air (*3*). This resulted in hydrogen-air explosions in reactors 1-3, a very energetic reaction which blew off the roof (Figure 2).

To further complicate matters and escalate the disaster, nuclear meltdowns occurred in reactors 1, 2, and 3. The fuel rods reached such a high temperature that they literally melted down through the base of the reactor. This was not confirmed until recently, using a new process known as muon tomography. The results of several months of these measurements indicated a shocking result: the reactor is empty. This points towards a complete reactor melt-out, where the fuel rods reached such a high temperature that it melted a hole through the reactor base, and escaped into the surroundings.

Figure 2: Hydrogen explosion in the Fukushima Reactor (*4*)

2 Muon Tomography Concept

There are two main methods for imaging using cosmic muons, one is via detecting muon transmission, and the other is by muon scattering.

The muon transmission method works by utilising the fact that cosmic muons are MIPs (Minimum Ionising Particles) which lose a set amount of energy as it travels through a medium: 2 MeV cm^{-1} for a material which has a density of 1 g cm^{-3} (*5*). The energy of the transmitted muons are measured, and a density map is built of the object being imaged. By taking density maps from various angles around the object, they are interpolated to reconstruct a 3D structure. This method is usually used for objects which are too large to build an entire detector system around, and also which have a relatively constant material density composition e.g. volcanoes.

The muon scattering method works by having detectors on both sides of the object, and tracking both the incoming and outgoing trajectories of the muons. This allows the generation of a much more accurate density map compared to muon transmission, which relies only on outgoing muons and not matching the data to the muons entering the object of interest. The angle the muons are scattered by is highly proportional to the atomic number of the material, where high-Z objects cause a significantly larger scattering angle compared to low-Z (Equation 2). This is particularly helpful when we are looking for something with a very different atomic number compared to its surroundings/background e.g. nuclear reactors.

2.1 Energy Loss

When a particle has an interaction with a material, there is often some energy loss occurring. There are two main processes by which the particle loses energy: Ionisation, where charged particles knock out electrons in the atoms of the target material, and energy is transferred. The other main energy loss avenue is Bremsstrahlung (literally german for ”braking rays”), also known as radiative losses: where a particle passes through the electromagnetic fields of atomic nuclei and emits radiation - commonly X-rays.

The energy lost per unit distance by a particle in a medium is given by the Bethe-Bloche formula (*6*), where r_e is the electron radius, m_e is the electron mass, β is the muon speed, N_A is Avogadros number, and Z is the atomic number.

$$\frac{dE}{dx} = 2\pi r_e^2 m_e c^2 \frac{z^2}{\beta^2} \frac{N_A Z_\rho}{A} \Big[ln(\frac{m_e c^2 \beta^2}{I(1-\beta^2)} - 2\beta^2)\Big] \propto \frac{1}{\beta^2} \tag{1}$$

For high energy particles, meaning relativistic particles with their kinetic energy being far higher than their rest mass energy, $\beta \approx 1$. This indicates that the loss in energy is minimal as the particle passes through a material. These are known as MIP (Minimum Ionising Particle), and they lose roughly 2 MeV cm^{-1} in a material with a density of 1 g cm^{-3}.

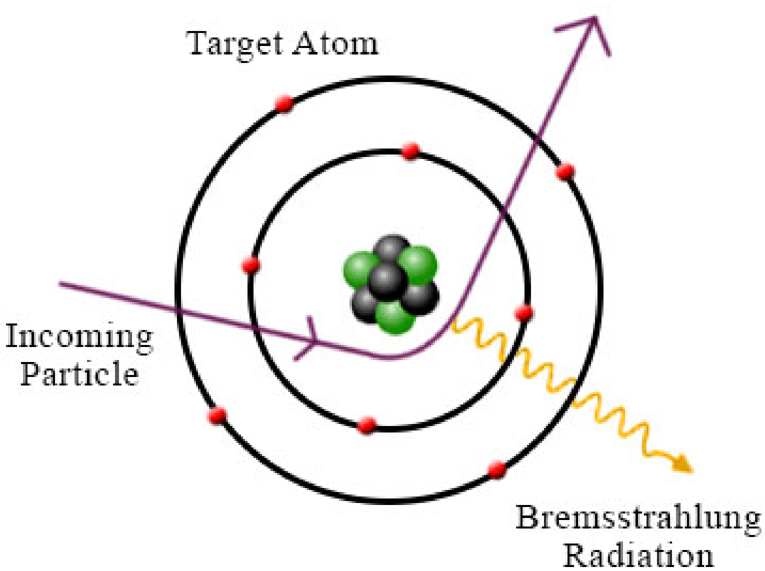

Figure 3: Illustration of an incident muon interacting with an atom and emitting Bremsstrahlung radiation.

2.2 Multiple scattering

The angle by which the muon is scattered when it passes through a medium, is given by the Fermi Approximation (*7*):

$$\theta_0 = \frac{14.1MeV}{p\beta}\sqrt{\frac{l}{X_0}} \tag{2}$$

Where θ_0 is the scattering angle, p is the muon momentum, v is the velocity, l is the length the muon passes through the material, and X_0 is the radiation length of the material.

$$\frac{dN}{d\theta} = \frac{1}{2\pi\theta_0^2}e^{-\frac{\theta^2}{2\theta_0^2}} \tag{3}$$

Where θ_0 is the multiple scattering angle and θ is the polar angle. The multiple scattering angle is defined by:

It is found that the scattering angles obey a Gaussian distribution, which is quite useful for simplifications and computing simulations. The Gaussian distribution function is defined as:

$$P(x) = \frac{1}{\sqrt{2\pi\sigma^2}}e^{-\frac{(x-\mu)^2}{2\sigma^2}} \tag{4}$$

Where μ is the expectation value (which is the mean, mode and median for a normal distribution), σ is the standard deviation, and σ^2 is the variance.

By inspection of the two equations 3 and 4 one can observe that they do indeed follow the same form.

3 Usage in Fukushima Daiichi

In December 2011 the Japanese government announced plans for a cold shut down of the reactor in preparation for decomissioning. In order to do so, knowledge of the situation of the reactor facility is necessary. The most important aspect of this, is the precise location of hazardously radioactive uranium fuel. The radiation levels reach such high levels that not only can no humans go near the area to perform measurements, even cameras get harmed by the severe intensity of the radiation, resulting in corruption of image data. Muon tomography allowed a way to non-invasively image the reactor and reactor core from a safe distance.

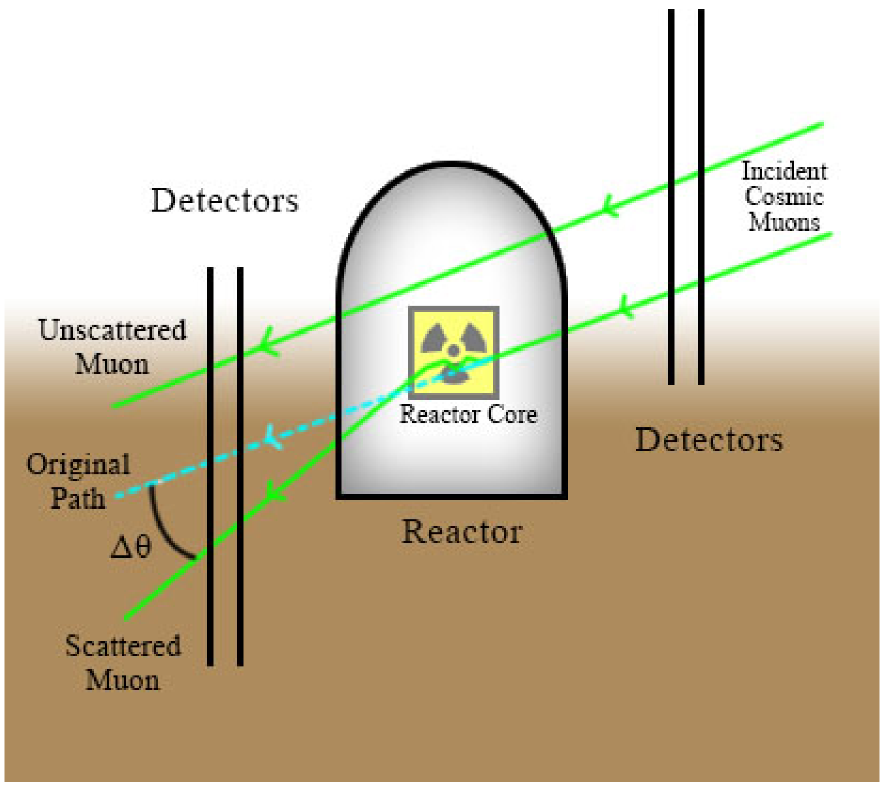

Figure 4: Diagram showing how the reactor was imaged.

3.1 Detector setup

The imaging system is formed of two square gas muon detectors, each 7 metres by 7 metres (*8*), placed on either side of the reactor. The core component is the aluminium gas-filled ionisation drift tubes (*9*). These detectors have a tracking efficiency higher than 99.7%, and have angular resolutions of 2 milliradians (*10*). Inside the gas drift tubes, the muon triggers an electromagnetic shower, which is detected and sent to the amplifier. From there, the DAQ takes over.

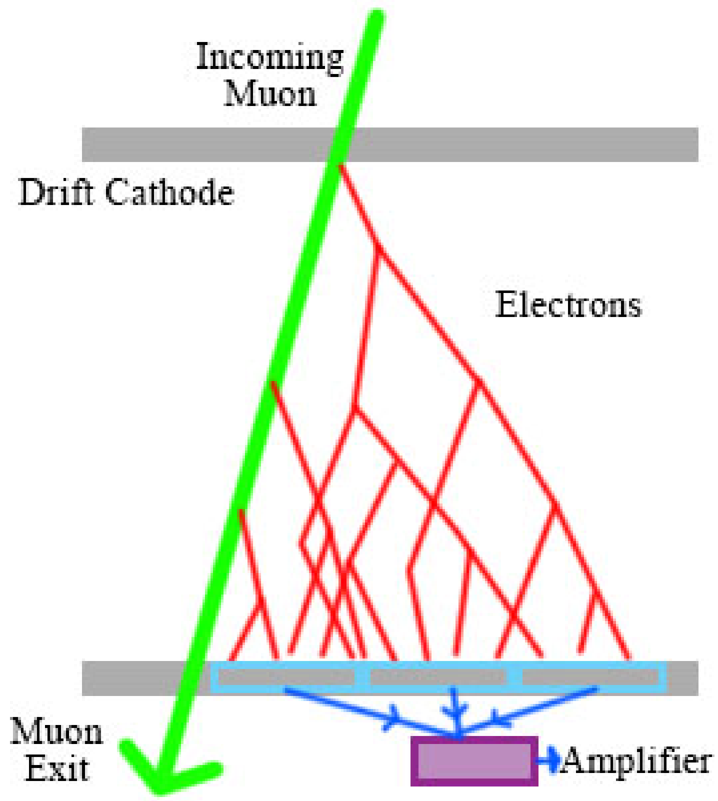

Figure 5: Diagram of the electron shower initiated by the muon passing through the gas drift tube.

3.2 Data Acquisition

The separate detectors track the incoming and outgoing muons, and send a pulse indicating that a muon has passed through a particular place at some time. Pulses from the drift tubes are then amplified for denoising, then digitised via FPGAs (Field Programmable Gate Array) TDCs (Time to Digital Converters) (*11*). The data is then sent via a dedicated ethernet connection to an array of computer clusters. By analysing this and after removing background noise, and matching up the tracks for a specific muon, the algorithm constructs a muon track vector of the respective trajectories (*11*), and thereby calculate the angular deviation of the muon - which is the angle the particle was scattered by. This data is then aggregated on a computer database, and analysed: regions that indicate a large scattering are highlighted as likely zones containing uranium.

3.3 My Simulation of muon detection

Since uranium and other fissile material is generally stored in cylindrical form, the distance of the muon will be the thickness of the cylinder as a chord. To find this we begin with the equation for a circle:

$$x^2 + y^2 = r^2 \tag{5}$$

And then rearrange it to find the distance the muon will pass through as some horizontal distance from the cylinder diameter. For simplicity purposes the incoming muon trajectory is modelled as orthogonal to the detector plane.

$$d = 2 \times \sqrt{\left(\frac{r}{x}\right)^2 - \left|\frac{y}{2r} - \left(\frac{r}{x}\right)^2\right|^2} \tag{6}$$

Where d is the distance the muon travels at a particular perpendicular distance from the axial diameter. Thus, we expect a larger amount of events detected around the centre of the uranium core, and less at the edges (where the muon has less distance travelled through high Z material).

The simulations are done with dimensions of 100x100 cm for the core, and 300x300 cm for the housing. As time passes it becomes clear that the uranium causes many more significant scattering events, compared to concrete.

Link to the source code I wrote for the basic simulator:

`https://pastebin.com/1a42geyS`

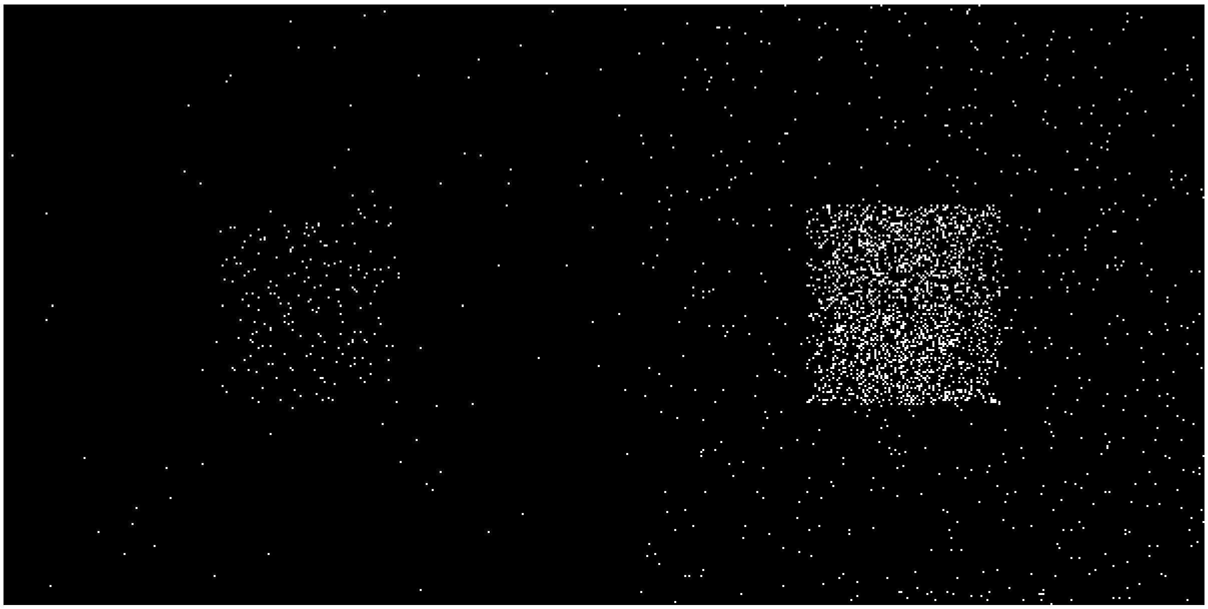

Figure 6: My simulations of muon detection over 100 seconds (left) and 1000 seconds (right)

4 Other uses of Muon Tomography

4.1 Nuclear Waste Imaging

Using muon radiography, nuclear waste material containers can be inspected for leaks. This is a risky job which can be harmful to radiation workers, and the non invasive procedure allows researchers to inspect the structural integrity of nuclear waste storage safely.

4.2 Non Proliferation: Smuggling Detection

The Decision Sciences International Corporation has developed the MMPDS (Multi-Mode Passive Detection System) which can detect illegal fissile material being transported discreetly. The advantage is that even radioactive shielding cannot hide the presence of the high-Z elements, as the muon passes right through it and shows the scattering. The detection process can be completed within a few minutes, as very highly detailed images are not necessary - just to indicate the presence of a high-Z material. Then the container/transport can be inspected manually.

4.3 Volcano structure

In some areas of the world that have high tectonic movement, volcanic activity is a reasonable cause for concern. Volcanologists would like to make forecasts and predictions regarding volcanic dormancy, and more importantly for the likelihood of an imminent eruption. A major indicator is the magma levels and reserves inside the magma chamber - a place where it is nigh impossible to inspect due to elevated risk to personell life. Muon transmission tomography is used to generate a 3d map of the volcano, a relatively safe method that collects data while the researchers are at a distance.

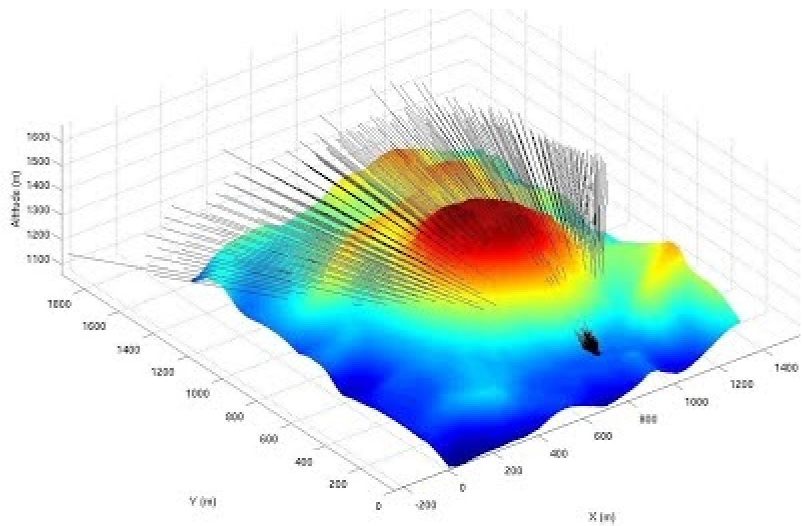

Figure 7: Density muon radiography of La Soufriere of Guadeloupe volcano (*12*)

5 Conclusion

The discovery of the new imaging technology poses vast implications for science, opening up a whole new set of possibilities. Not only is it bringing many new discoveries to light, but also the applications it is currently used in are saving many lives, and have the potential to save many more. In Fukushima, it has demonstrated that a substantial quantity of the reactor core material has fully escaped from the reactor bounds, and has been distributed around the region.

References and Notes

1. P. Y. Lipscy, K. E. Kushida, T. Incerti, *Environmental science & technology* **47**, 6082 (2013).

2. J. M. Agency .

3. P. Matanle, *Local Environment* **16**, 823 (2011).

4. D. M. Arkadiusz Podniesiski, *The Asia-Pacific Journal* **14**, 1098 (2016).

5. D. R. Corson, R. B. Brode, *Physical Review* **53**, 773 (1938).

6. J. Pitarke, R. Ritchie, P. Echenique, E. Zaremba, *EPL (Europhysics Letters)* **24**, 613 (1993).

7. A. Aguilar-Arevalo, *et al.*, *Physical review letters* **100**, 032301 (2008).

8. J. M. Durham, Imaging the core of fukushima reactor with muons, *Tech. rep.*, Los Alamos National Lab.(LANL), Los Alamos, NM (United States) (2015).

9. Z. Wang, *et al.*, *Nuclear Instruments and Methods in Physics Research Section A: Accelerators, Spectrometers, Detectors and Associated Equipment* **605**, 430 (2009).

10. R. Barate, *et al.*, *Physics Reports* **294**, 1 (1998).

11. H. Miyadera, *et al.*, *Aip Advances* **3**, 052133 (2013).

12. N. Lesparre, *et al.*, *Geophysical Journal International* **190**, 1008 (2012).